Brain Structure and Function (2019) 224:1447–1455
https://doi.org/10.1007/s00429-019-01849-1

ORIGINAL ARTICLE

Parcellation of motor cortex-associated regions in the human corpus callosum on the basis of Human Connectome Project data

Martin Domin[1] · **Martin Lotze**[1]

Received: 22 August 2018 / Accepted: 11 February 2019 / Published online: 18 February 2019

Abstract

The corpus callosum (CC) is the largest white matter structure of the brain and offers the structural basis for an intense interaction between both cerebral hemispheres. Especially with respect to the interaction of both motor cortices it shows a differentiated somatotopic organization. Neuropathological processes are often reflected in structural alterations of the CC and a spatially precise description of structures for the healthy brain is essential for further differentiation of structural damage in patients. We performed a fine-grained parcellation of the CC on 1065 diffusion-weighted data sets of the Human Connectome Project. Interhemispheric tractograms between interhemispherically corresponding functional subdivisions of the primary motor cortex (M1; Brainnetome Atlas) were calculated, transformed into a common space, averaged and thresholded, to be assessed for localization, fractional anisotropy (FA) and mean diffusivity (MD). Spatially distinct CC regions for each functional M1 subdivision (lower and upper limbs, head/face, tongue/larynx) were identified and will be available as anatomical masks. Non-parametrical statistics for the average FA and MD values showed significant differences between all callosal regions. The newly proposed callosal regions allow for a precise differentiation of M1–M1 motor connectivity and the structural integrity of these tracts. Availability of masked regions in a common space will help to better understand inter-hemispherical callosal connectivity in patients or healthy volunteers.

Keywords Corpus callosum · Motor cortex · DTI · Probabilistic tractography · Parcellation · Human Connectome Project

Introduction

As a distinct brain feature, the corpus callosum (CC), also known as the callosal commissure, contains the largest amount of white matter connecting both cerebral hemispheres. Topological models describe this structure as a medial white matter bundle, entering from cortical areas of one hemisphere and terminating in homologous or heterotypical areas of the other hemisphere (Witelson 1989; Clarke and Zaidel 1994). A large amount of studies have been conducted, evaluating the relationship of neuropathology and neuromorphology of the CC, for syndromes such as dyslexia (Hynd et al. 1995), schizophrenia (Brambilla et al. 2005), attention-deficit hyperactivity disorder (ADHD) (Skranes et al. 2007), stroke (Li et al. 2015) or neurodegenerative diseases like multiple sclerosis (Wahl et al. 2011). To further improve the structural evaluation of the CC concerning normal, e.g., age-related, or pathological changes, a segmentation into subdivisions as precise as possible could be of great value.

Although the microscopic fiber structure of the CC can be seen as rather heterogeneous, no visible landmarks or compartments at the macroscopic scale can be identified (Chao et al. 2009; Cover et al. 2017). Numerous approaches have been proposed to subdivide the CC into spatial distinct regions, relying on postmortem (Witelson 1989) and subsequent microscopic analyses (Aboitiz et al. 1992).

Using diffusion-weighted imaging (DWI), characteristically well-oriented fibers perpendicular to the mid-sagittal plane can be exploited to generate a good tissue contrast between the CC and other cerebral structures. DWI is based on the measurement of water diffusion and reveals the major orientation of white matter fiber tracts on the macroscopic level by using streamline tractography (Behrens et al. 2007). However, due to the missing landmarks, a subdivision of the CC remains challenging and up to present, a gold standard

✉ Martin Domin
martin.domin@uni-greifswald.de

[1] Functional Imaging Unit, Institute of Diagnostic Radiology and Neuroradiology, University Medicine Greifswald, Walther- Rathenau-Str. 46, 17475 Greifswald, Germany

or validation metrics are lacking for assessing the quality of a certain parcellation strategy. Besides of cadaver studies multiple DWI-based approaches evaluated structural connectivity between cortical regions connected via fiber tracts running through the CC (Cook et al. 2005; Huang et al. 2005; Hofer and Frahm 2006; Park et al. 2008; Chao et al. 2009; Lebel et al. 2010; Schulz et al. 2015) or applied data-driven methods such as watershed transformation (Rittner et al. 2014; Cover et al. 2017).

Overall, connectivity-based methods are highly dependent on the anatomical references used and the lower the spatial resolution of the reference system the less accurate is the differentiation of the structure investigated. Data-driven approaches provide local differences in fiber tracts, but no understanding of their affiliation to functional subsystems.

For the motor domain, the CC participates in function such as interhemispheric interaction for bilaterally represented movements for instance of the face and tongue representation, interhemispheric interaction for precise coordination of bilaterally performed movements for instance for the upper and lower limb, or cortical inhibition of unilaterally represented movements from the contralateral to ipsilateral hemisphere for instance for the upper limb (Grefkes et al. 2008). A subdivision of somatotopically different subunits can be derived by combining functional datasets with DWI-measures in the MNI space. Both, a high quality of DWI measures and functional representation maps are available in the Human Connectome dataset for a sufficiently powered sample (1065 healthy participants) and the Brainnetome Atlas, respectively. We here used a connectivity-based approach combined with functional seeds on this dataset to evaluate four different subdivisions of the CC with respect to their functional representation. In addition, we compared spatial distinctiveness of these subunits statistically. This procedure uses state-of-the-art methods to provide CC regions of interest in the MNI space for further analyses in other cohorts.

Methods

Data acquisition

Diffusion-weighted scans were collected by the Human Connectome Project (HCP); (http://www.cmrr.umn.edu/multiband). From these data those of the "HCP young adult" study were used, comprising 1200 subject data sets, of which 1065 contained valid diffusion-weighted MRIs (dMRI). The subjects' ages ranged from 22 to 35 years (mean = 28.75 ± 3.67 years), 575 were female and 490 male.

Diffusion MRI data comprised three different gradient tables, with each table acquired once with right-to-left and left-to-right phase-encoding polarities. Each of the gradient tables included 90 diffusion weighting directions plus 6 $b = 0$ acquisitions interspersed throughout each run. Diffusion weighting consisted of 3 shells of $b = 1000$, 2000, and 3000 s/mm^2 interspersed with an approximately equal number of acquisitions on each shell within each run. The diffusion directions were obtained using a toolbox available from INRIA that returns uniformly distributed directions in multiple q-space shells. The directions are optimized so that every subset of the first M directions is also isotropic (Glasser et al. 2013).

The following global scan parameters for the multi-band diffusion sequence were used: voxel size = 1.25 mm^3, slices = 111, TR = 5520, TE = 89.5 resulting in a scan time of 9:41 min for each acquisition. For in-depth description of the sequences used see the Reference Manual of the HCP (WU-Minn HCP 1200 Subjects Release: Reference Manual –>Appendix I—Protocol Guidance and HCP Session Protocols–> Diffusion Session).

Preprocessing

FMRIB's software library 5 (FSL 5) (Jenkinson et al. 2012) was used to correct for distortions caused by susceptibility (FSL TOPUP) and eddy-current-induced artifacts (FSL EDDY). Whereas susceptibility-related artifacts are constant in a spatial manner throughout the measurement, eddy-current-induced distortions are unique for every diffusion-weighted volume (Andersson and Sotiropoulos 2016). The estimation (and correction) of susceptibility-induced distortions takes advantage of the complementary information included in pairs of diffusion images acquired with reversed phase-encoding (PE) directions. Reversing the PE direction flips the sign of susceptibility-induced distortions as well and the combination of both images allows for estimation of an off-resonance field. In the HCP processing pipeline only the estimation takes place, as the field map is fed into the subsequent stage that estimates the eddy-current induced distortions and motion-related artifacts. For this step the complementary information of two nearly opposing diffusion gradient directions were used, as they are expected to exhibit nearly opposite eddy-current induced distortions, whereas susceptibility distortions remain unchanged. With the previously built field map as a starting point these data were fed into a Gaussian Process predictor, used to additionally estimate the eddy-current induced field and the subject motion for each diffusion-MRI volume. The estimated field maps were combined and used to correct the volumes in a single resampling step and spline interpolation (Andersson et al. 2012).

Fiber orientation density function estimation

We chose the ball and stick model of FSL BEDPOSTX (Behrens et al. 2003) for inferring the fiber orientation density function (fODF) from diffusion MRI. In addition, for the HCP data this approach was extended via a parametric deconvolution to take full advantage of the multi-shell data with different diffusion weightings (*b*-values). The fiber orientations and their uncertainty were estimated using Bayesian inference on the multi-shell spherical deconvolution framework and a Rician noise model (Jbabdi et al. 2012). The number of fiber compartments in each voxel was determined using automatic relevance determination (ARD) priors, as suggested by Behrens and colleagues (Behrens et al. 2007). For further details and in-depth description of the preprocessing pipeline see Sotiropoulos et al. (2013).

Tractography and parcellation

Diffusion-MRI related tractography describes a technique to model tracks or streamlines in a three-dimensional vector field, the vectors describing the primary direction of water diffusion and in the case of, e.g., the enhanced ball and stick model, multiple differently weighted directions per voxel are possible. Here, the FSL PROBTRACKX approach was used, which repetitively samples from the posterior distribution on principal diffusion directions and progresses along this same direction. By taking many such samples a connectivity distribution is build up, depicting a frequency map, where every voxel encodes the sum of streamlines running through this voxel.

For the tractography-related seed ROIs of the primary motor cortex (M1) we used the Brainnetome Atlas (BNA) (Fan et al. 2016) (http://atlas.brainnetome.org). In particular, the following ROIs of the M1 were extracted that are related to certain motor functionality: head/face (A4hf), tongue/larynx (A4tl), upper limbs (A4ul) and lower limbs (A4ll), each for the left and right hemisphere (Fig. 1). Additionally, the JHU ICBM-DTI-81 White-Matter Labels atlas (Mori et al. 2005) was used to extract a ROI of the corpus callosum.

Tractography took place in the space of the individual data set in order to avoid problems by normalization of the DWI-dataset into the MNI space. Therefore, the extracted ROIs were transformed from ICBM MNI152 space to the individual data, which was done via the nonlinear warp field included in every individual data set. FSL's APPLYWARP was used, with nearest-neighbor interpolation and intermediary supersampling enabled to minimize changes of the anatomical configuration in the course of the transformation.

FSL PROBTRACKX was configured in a start-waypoint-fashion, e.g., the ROI for the upper limbs region on the left hemisphere acted as a seed region, the CC and upper limbs region on the right hemisphere (in this order)

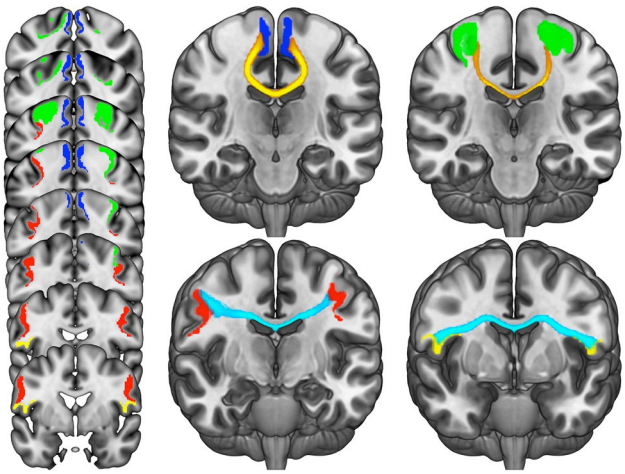

Fig. 1 Left column: depiction of seed regions used for tractography (regional color coding: lower limb = blue; upper limb = green; head/face = red; tongue/larynx = yellow). Middle and right column: population-wise inter-hemispherical tractograms (cyan/orange) between each pair of homologous seed regions (same regional color coding as on the left side of the figure)

as waypoint ROIs. Additional parameters included loop check (-l), modified Euler streamlining (--modeuler), curvature threshold (-c 0.2), number of steps per sample (-S 2000), step length in mm (--steplength = 0.5), number of samples (-P 5000) and the rejection of streamlines that do not hit waypoints in the given order (--wayorder). Defaults were used otherwise. For every region two tractograms were calculated, using either the left or right hemisphere as the starting side, to take into account the inherent hemispherical asymmetry of the human brain. Even in subject space the process of tractography accumulated to a vast amount of processing time wherefore the local high performance cluster was used to calculate the tractograms.

Post-processing of the tractograms included scaling of voxel values by seed ROI size and by the waytotal value (total number of successful streamlines) and nonlinear transformation into MNI template space, using the warp fields included in the HCP data. All transformed tractograms that belong to a certain seed–waypoint combination, were added up voxel-wise. As the tractograms were calculated for left and right hemispheres separately, an average sum tractogram for each M1 subregion was created, depicting the connection between a certain subregion on both hemispheres running through the CC. Due to the individual spatial variance each sum tractogram shows a spatially widespread connectivity, which was therefore thresholded to both 25% and 50% of the maximum connectivity value. This spatial variance reduction identifies dominant connectivity structures for each callosal subregion. Figure 2 summarizes the data processing pipeline.

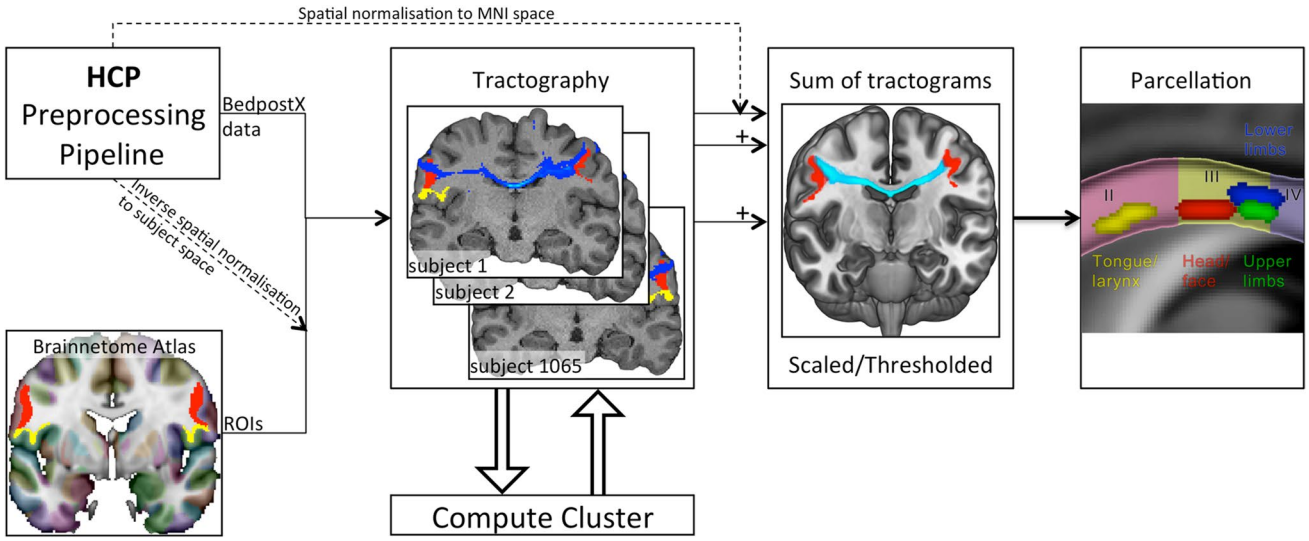

Fig. 2 Flowchart of the tractography-based generation of a callosal parcellation. 1065 preprocessed datasets of the HCP were used to calculate inter-hemispherical probabilistic tractograms between ROIs of both left and right primary motor cortices (Brainnetome atlas: sub regions of Brodmann area 4). After transformation to MNI template space the sum of these tractograms highlights the motor regions of the corpus callosum

Statistical procedures

FSL's DTIFIT was used to calculate maps for fractional anisotropy (FA) and mean diffusivity (MD) for every subject. Since the callosal subregions were created in the MNI template space, a spatial transformation into individual subject space had to be performed in the same way as already described above. The calculated diffusion index maps were multiplied by each de-normalized probabilistic callosal subregion, producing a masked map for each subregion and diffusion index. The mean values of each masked map represent a weighted mean, taking into account the probabilistic nature of the callosal parcellation.

A related-samples Friedman's two-way analysis of variance by ranks (FA and MD values were not normally distributed) was conducted as the non-parametrical alternative to a one-factor repeated-measures ANOVA (IBM SPSS Statistics v20) to evaluate the influence of the spatial position of the proposed parcellation on fractional anisotropy and mean diffusivity. Post hoc analyses were performed using Wilcoxon signed-rank tests (Bonferroni corrected).

For analysis of spatial and quantitative distinctiveness of each of the proposed callosal subregions, we calculated the peak frequency value for each sagittal slice (x-direction). For each sagittal slice the corresponding peak value coordinates were used to determine the Euclidean distances between all possible combinations for these points, by calculating the absolute value of the vector between two points. For each combination, the Euclidean distances were used to determine the spatial difference between the peak value streamlines. Here, we set a threshold distance between the dominant streamlines of the tractograms, which could be defined as "at least one voxel apart" ($\sqrt{1\ \text{mm}^2 + 1\ \text{mm}^2}$) or, more conservative, "at least one voxel between two coordinates" ($\sqrt{2\ \text{mm}^2 + 2\ \text{mm}^2}$).

Results

The proposed method resulted in a spatially distinct parcellation of the CC with an anterior subdivision for the tongue/larynx cortical areas, a medial subdivision for the head/face cortical areas and posterior subdivisions for the limbs (lower limbs more superior to upper limbs; see Fig. 3). When comparing our results to most recent tractography-based parcellation (Chao et al. 2009; based on: Witelson 1989), our callosal regions were located in the parcels II and III. In more detail, the tongue/larynx and head/face associated cortical regions were located in parcel II, lower and upper limbs in parcel II and III (Fig. 3).

Table 1 shows descriptive values for FA and MD of each callosal subregion.

FA of subregions were highest for lower limbs (0.51 ± 0.036), followed by upper limbs (0.45 ± 0.034) and lowest for tongue/larynx (0.41 ± 0.029) followed by head/face (0.45 ± 0.037). Both, fractional anisotropy (FA: $\chi^2(3) = 2411.71$, $p < .001$) and mean diffusivity (MD: $\chi^2(3) = 2461.05$, $p < .001$) differed between the proposed callosal subregions. Post hoc analysis revealed significant differences in FA and MD between all paired subregions (Table 2).

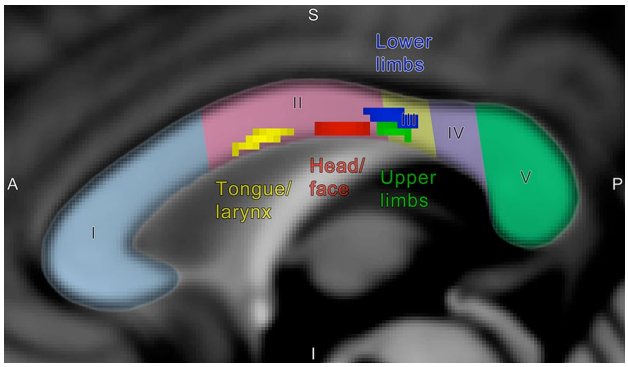

Fig. 3 Callosal subregions (tongue/larynx, head/face; lower limb, upper limb) as identified by our study in comparison to the tractography-based parcellation by Chao et al. (2009; parcel I–V). All maps where overlaid on the ICBM MNI152 nonlinear 6th generation template brain and magnified to emphasize the corpus callosum in midsagittal plane. *A* anterior, *P* posterior, *S* superior, *I* inferior

Mean spatial distinctiveness for each proposed callosal subregion as measured by Euclidean distances between the frequency peak values are plotted in Table 3. Additionally, all paired peak value coordinates showed medium to strong differences following the "at least one voxel apart" criterion defined in the "Method" section. Visualizing the peak value streamlines of the different functional somatotopic seeds showed a clear spatial distinctiveness as depicted in Fig. 4.

Discussion

The current study represents a consequential progression of previous works by utilizing the, up to now, best available dataset containing high-resolution diffusion-weighted brain data, improved by state-of-art preprocessing. By incorporating a detailed atlas for the primary motor cortex we here propose an equally fine-grained parcellation of the corpus callosum. The four M1-regions of the Brainnetome Atlas (upper limbs, lower limbs, head/face, tongue/larynx) resulted in four subregions, which are distinct when differentiated by peak value coordinates, but partially located closely nearby (Euclidean distances: 2.46–20.49 mm). This finding necessitates high spatial DWI-resolution for such subdivision analyses.

Importance of the precentral gyrus

We here focused on the M1-transcallosal fibers, because of their relevance to a number of clinical approaches. For instance stroke, as a major cause of chronic disability in western community, shows a high rate of motor function impairment. Here, DWI-parameters are important biomarkers for current and later impairment, e.g., hand function (Lindow et al. 2016) or dysphagia (Mihai et al. 2016) and might even help for selection of appropriate interventions (Horn et al. 2016; Lotze et al. 2017). In addition, light microscopic approaches identified large diameter fibers for

Table 1 Descriptive statistics of each proposed callosal subregion for the diffusion tensor parameters mean diffusivity (MD) and fractional anisotropy (FA)

Subregion	MD mean	MD std. deviation	95% confidence interval for MD mean		FA mean	FA std. deviation	95% confidence interval for FA mean	
			Lower	Upper			Lower	Upper
Head/face	0.000288	0.000015	0.000287	0.000289	0.4512	0.0366	0.4490	0.4534
Tongue/larynx	0.000243	0.000013	0.000242	0.000244	0.4131	0.0292	0.4114	0.4149
Lower limbs	0.000285	0.000013	0.000284	0.000286	0.5150	0.0364	0.5128	0.5172
Upper limbs	0.000297	0.000015	0.000296	0.000298	0.4478	0.0341	0.4457	0.4498

Table 2 Statistical values for the differences between paired subregions are provided as results of the post hoc Wilcoxon signed-rank tests for differences of callosal diffusion tensor parameters MD and FA

Pairs	MD: paired differences			FA: paired differences		
	Wilcoxon *z*	*p* (Bonf.)	Cohen's *r*	Wilcoxon *z*	*p* (Bonf.)	Cohen's *r*
Lower limbs—head/face	− 9.146	< 0.001	0.28	− 27.91	< 0.001	0.86
Lower limbs—tongue/larynx	− 28.272	< 0.001	0.87	− 28.23	< 0.001	0.87
Tongue/larynx—head/face	− 28.273	< 0.001	0.87	− 26.45	< 0.001	0.81
Upper limbs—head/face	− 21.394	< 0.001	0.66	− 4.71	< 0.001	0.14
Upper limbs—lower limbs	− 25.765	< 0.001	0.79	− 28.03	< 0.001	0.86
Upper limbs—tongue/larynx	− 28.272	< 0.001	0.87	− 25.36	< 0.001	0.78

Table 3 Mean Euclidean distances, given in mm, between paired subregions

Pairs	Mean Euclidean distances (mm)	Euclidean distance Std. Dev. (mm)	95% Confidence interval for Euclidean distance	
			Lower	Upper
Lower limbs—head/face	7.99	1.34	7.56	8.42
Lower limbs—tongue/larynx	20.19	1.39	19.74	20.63
Tongue/larynx—head/face	12.28	0.73	12.05	12.51
Upper limbs—head/face	7.24	0.97	6.93	7.54
Upper limbs—lower limbs	2.46	1.03	2.13	2.79
Upper limbs—tongue/larynx	19.43	0.77	19.18	19.68

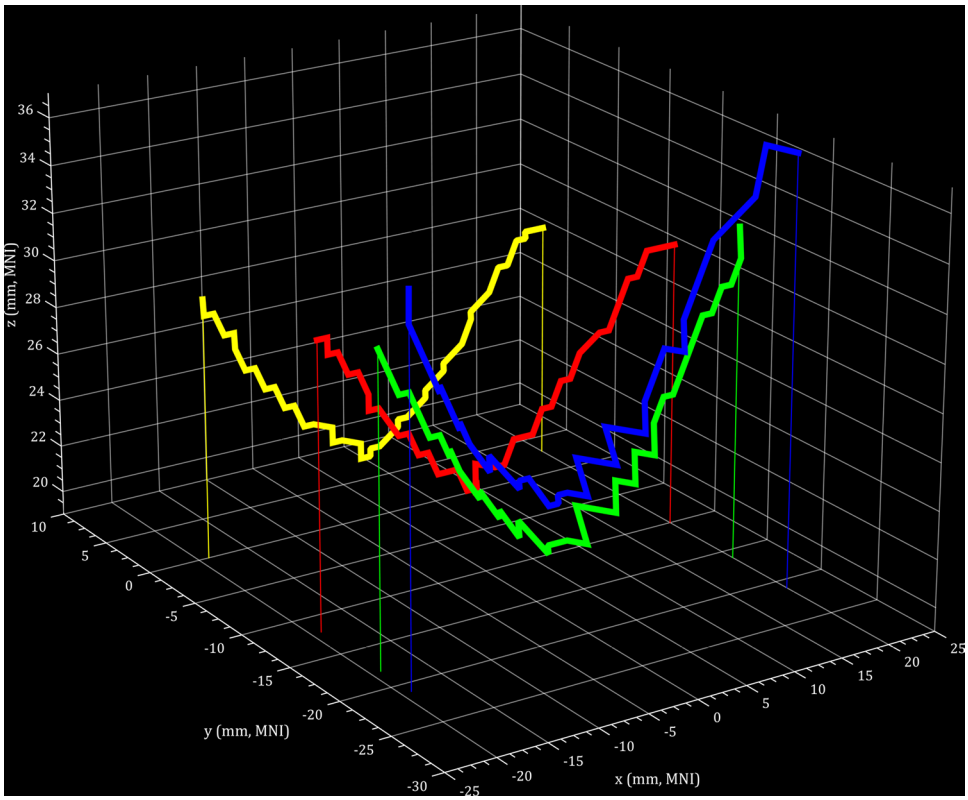

Fig. 4 Frequency peak value streamlines of each proposed callosal subregion (blue = lower limbs; green = upper limbs; red = head/face; yellow = tongue/larynx; MNI space units in mm)

the sensorimotor system but smaller for prefrontal areas and association areas (Aboitiz et al. 1992), making a DWI-approach in this region of the CC more suitable. Previous research groups investigated connectivity-based parcellation of the CC for the entire precentral sulcus (Hofer and Frahm 2006; Park et al. 2008; Chao et al. 2009) or the entire pre- and postcentral gyrus (Cover et al. 2017). Instead, we defined functionally differentiated subregions within M1 since it can be expected that transcallosal fibers between functional subareas do substantially differ [different functional interaction between bilaterally represented trunk or head-related movements and unilateral represented movements of extremities (Wassermann et al. 1991)]. A differentiated parcellation of the CC allows for more specialized assessments of motor function impairments, as for the first time it will be possible to examine the influence of, e.g., stroke incidents on interhemispheric white matter connectivity on a granular level. Dysphagia after stroke as a common and potentially life-threatening consequence can now be assessed in more detail, similarly the hemiparesis of extremities, since each functional cortical representation of the motor cortex is now accessible on a distinct structural connectivity level.

Spatial resolution

This subdivision of M1 necessitates high resolution of both DWI measurement and methods for data evaluation and

assignment to an atlas. Any previously created CC parcellation was constrained by the low spatial resolution of the included diffusion-weighted data (Park et al. 2008; Chao et al. 2009). Additionally, the much coarser cortical parcellations of the previously employed brain atlases, especially for the motor cortex, further impeded detailed subdivisions and therefore preceding studies represent only minor alterations in comparison to each other. In this context, it has to be noted that a constant increase in resolution could introduce new issues, e.g., registration difficulties or biological differences becoming more prominent, resulting in increasingly varying locations of region boundaries with a higher likelihood of changing source, location or target of individual reconstructed white matter fiber tracts (de Reus and van den Heuvel 2013). Due to the high quality of the HCP data many of these issues can be minimized, for instance illustrated by each subject's contribution to the dominant group connectivity distributions and the related low inter-individual variability. Here, for each investigated tractogram a very high amount of subjects contributed to the same MNI coordinates of the dominant parts of the reconstructed fiber tracts [head/face area 1044 /1065 (98%), lower limbs area 1065/1065 (100%), tongue/larynx area 1017/1065 (95.5%), upper limbs area 1047/1065 (98.3%)]. This demonstrates the anatomical spatial stability of the connections and the high quality of the spatial normalization of the datasets, which results in a very good structural alignment between datasets.

Differentiation of the anatomy of the CC

A subdivision of the CC solely on classical anatomical criteria seems not fully appropriate for the in vivo investigations performed on large samples nowadays. For instance the Witelson method (Witelson 1989), as one of the first description for subdividing the CC and used even today, is not based on MNI or Talairach brain coordinates. This method has been criticized earlier already (Hofer and Frahm 2006). Since the cuts between segments are arbitrarily performed (without AC–PC-alignment), this method does not subdivide the CC on a simple coronal plane, but into oblique sections. It is time now to subdivide the CC in a MNI-oriented way with differentiation of functional subdivisions and not by macroscopic gyral structure, which shows high inter-subject variability in functional representation. Aboitiz and colleagues (Aboitiz et al. 1992) illustrated in their work the heterogeneous architecture of the CC. By counting fibers of different diameters and calculating the regional density of these different fibers they were able to provide callosal fiber density profiles. Their conclusion implies that there are larger proportions of large diameter fibers in callosal regions that interconnect primary sensory or perhaps motor areas than in regions that interconnect association and prefrontal areas. Fibers with larger axon diameters will have substantially more radial water diffusion, lowering diffusion properties like FA, which corresponds to the highly significant differences of the proposed subregions. The lower limbs area therefore represents by its highest FA of all four regions the highest integration and density of thinner fibers, whereas the tongue/larynx area contains the lowest FA value, upper limbs and head/face areas in between. One explanation could be the varying necessary interhemispherical communication for efficient motor function execution. More fibers with large diameters would be necessary for a faster communication between hemispheres while employing complex sensory tasks, which could be shown for the posterior midbody, where the highest density of large callosal fibers was found. Aboitiz et al. proposed that this region represents the connections between primary and secondary auditory cortices. Fast connections and the subsequent timing of the cellular response in each hemisphere are important for localizing sounds in space.

Limitations

Due to the high quality of the underlying data, many limitations that are known from other studies are minimized here. Particularly, issues like low angular diffusion direction resolution, low or high *b* values, low spatial resolution or small sample sizes are reduced or treated as best as currently possible in the sense of what advances in technology make possible. Nevertheless, some possible issues should be addressed here. At first, the demographic structure of the Human Connectome sample contains many relatives, siblings and a high number of genetic twin pairs. It could be assumed, that in genetic relationships and, especially, twins inherited structural similarities exist (Kochunov et al. 2010; Lee et al. 2015). It is beyond question, that genetic control over white matter structure exists, but the question remains about the tightness of this control. By performing subgroup analyses (twin vs. twin; twin pairs only; unrelated subjects only), no significant structural differences between groups could be found. The assessed regions in the CC showed no relevant spatial alterations. Surely, a more in-depth genetic analysis with proper data would be necessary, but this is not the scope of this manuscript.

A second, still unresolved issue resides in the decision of proper "thresholding" of the probabilistic tractograms, the When and the How. The approach described in this manuscript performs thresholding after averaging all individual tractograms, removing the noise and the inter-subject variance. Another way would be a thresholding on subject level, prior to averaging, using the same common thresholds of 25% and 50%. By performing a comparison of both approaches we could show, that no relevant difference in spatial location of the dominant peak value tracts exist. As the inter-subject variance is not known and hard to quantify,

an in-depth analysis could reveal more information on this issue, as it is still unclear, which thresholds should be used and why.

Conclusions

With the Human Connectome Project a spatially high-precision dataset in a sufficient sample size is available for the first time. This dataset will enable us to differentiate brain structures and structural as well as functional connectivity of the healthy human brain in a completely new quality. In addition, the usage of functional ROIs from a high-quality brain atlas offers unique possibilities to improve the investigation of interactions of brain function and structure.

The newly proposed callosal regions allow for a precise differentiation of M1–M1 motor connectivity and the structural integrity of these tracts in the human corpus callosum. As a publicly available dataset, these regions in the common MNI space will help to better understand inter-hemispherical callosal connectivity in patients or healthy subjects. A collection of probabilistic ROIs and tractograms can be found on the Internet, especially on GitHub (https://github.com/NitramNimod/CorpusCallosumParcellation).

Acknowledgements Diffusion-weighted images were generously provided by the courtesy of the Human Connectome Project. MD and ML were funded by the University Medicine Greifswald.

Compliance with ethical standards

Conflict of interest The authors declare no competing financial interests.

References

Aboitiz F, Scheibel AB, Fisher RS, Zaidel E (1992) Fiber composition of the human corpus callosum. Brain Res 598:143–153. https://doi.org/10.1016/0006-8993(92)90178-C

Andersson JLR, Sotiropoulos SN (2016) An integrated approach to correction for off-resonance effects and subject movement in diffusion MR imaging. Neuroimage 125:1063–1078. https://doi.org/10.1016/j.neuroimage.2015.10.019

Andersson JL, Xu J, Yacoub E et al (2012) A comprehensive Gaussian process framework for correcting distortions and movements in diffusion images. Proc Intl Soc Mag Reson Med 20:2426

Behrens TEJ, Woolrich MW, Jenkinson M et al (2003) Characterization and propagation of uncertainty in diffusion-weighted MR imaging. Magn Reson Med 50:1077–1088. https://doi.org/10.1002/mrm.10609

Behrens TEJ, Berg HJ, Jbabdi S et al (2007) Probabilistic diffusion tractography with multiple fibre orientations: what can we gain? Neuroimage 34:144–155. https://doi.org/10.1016/j.neuroimage.2006.09.018

Brambilla P, Cerini R, Gasparini A et al (2005) Investigation of corpus callosum in schizophrenia with diffusion imaging. Schizophr Res 79:201–210. https://doi.org/10.1016/j.schres.2005.04.012

Chao YP, Cho KH, Yeh CH et al (2009) Probabilistic topography of human corpus callosum using cytoarchitectural parcellation and high angular resolution diffusion imaging tractography. Hum Brain Map 30:3172–3187. https://doi.org/10.1002/hbm.20739

Clarke JM, Zaidel E (1994) Anatomical-behavioral relationships: corpus callosum morphometry and hemispheric specialization. Behav Brain Res 64:185–202. https://doi.org/10.1016/0166-4328(94)90131-7

Cook PA, Zhang H, Avants BB et al (2005) An automated approach to connectivity-based partitioning of brain structures. 164–171. https://doi.org/10.1007/11566465_21

Cover G, Pereira M, Bento M et al (2017) Data-driven corpus callosum parcellation method through diffusion tensor imaging. IEEE Access 5:22421–22432. https://doi.org/10.1109/ACCESS.2017.2761701

de Reus MA, van den Heuvel MP (2013) The parcellation-based connectome: limitations and extensions. Neuroimage 80:397–404. https://doi.org/10.1016/j.neuroimage.2013.03.053

Fan L, Li H, Zhuo J et al (2016) The human brainnetome atlas: a new brain atlas based on connectional architecture. Cereb Cortex 26:3508–3526. https://doi.org/10.1093/cercor/bhw157

Glasser MF, Sotiropoulos SN, Wilson JA et al (2013) The minimal preprocessing pipelines for the human connectome project. Neuroimage 80:105–124. https://doi.org/10.1016/j.neuroimage.2013.04.127

Grefkes C, Eickhoff SB, Nowak DA et al (2008) Dynamic intra- and interhemispheric interactions during unilateral and bilateral hand movements assessed with fMRI and DCM. Neuroimage 41:1382–1394. https://doi.org/10.1016/j.neuroimage.2008.03.048

Hofer S, Frahm J (2006) Topography of the human corpus callosum revisited-comprehensive fiber tractography using diffusion tensor magnetic resonance imaging. Neuroimage 32:989–994. https://doi.org/10.1016/j.neuroimage.2006.05.044

Horn U, Roschka S, Eyme K et al (2016) Increased ventral premotor cortex recruitment after arm training in an fMRI study with subacute stroke patients. Behav Brain Res 308:152–159. https://doi.org/10.1016/j.bbr.2016.04.040

Huang H, Zhang J, Jiang H et al (2005) DTI tractography based parcellation of white matter: application to the mid-sagittal morphology of corpus callosum. Neuroimage 26:195–205. https://doi.org/10.1016/j.neuroimage.2005.01.019

Hynd GW, Hall J, Novey ES et al (1995) Dyslexia and corpus callosum morphometry. Arch Neurol 52:32–38

Jbabdi S, Sotiropoulos SN, Savio AM et al (2012) Model-based analysis of multishell diffusion MR data for tractography: how to get over fitting problems. Magn Reson Med 68:1846–1855. https://doi.org/10.1002/mrm.24204

Jenkinson M, Beckmann CF, Behrens TEJ et al (2012) FSL Neuroimage 62:782–790. https://doi.org/10.1016/j.neuroimage.2011.09.015

Kochunov P, Glahn DC, Lancaster JL et al (2010) Genetics of microstructure of cerebral white matter using diffusion tensor imaging. Neuroimage 53:1109–1116. https://doi.org/10.1016/j.neuroimage.2010.01.078

Lebel C, Caverhill-Godkewitsch S, Beaulieu C (2010) Age-related regional variations of the corpus callosum identified by diffusion tensor tractography. Neuroimage 52:20–31. https://doi.org/10.1016/j.neuroimage.2010.03.072

Lee SJ, Steiner RJ, Luo S et al (2015) Quantitative tract-based white matter heritability in twin neonates. Neuroimage 111:123–135. https://doi.org/10.1016/j.neuroimage.2015.02.021

Li Y, Wu P, Liang F, Huang W (2015) The microstructural status of the corpus callosum is associated with the degree of motor function and neurological deficit in stroke patients. PLoS One 10:1–17. https://doi.org/10.1371/journal.pone.0122615

Lindow J, Domin M, Grothe M et al (2016) Connectivity-based predictions of hand motor outcome for patients at the subacute stage after stroke. Front Hum Neurosci. https://doi.org/10.3389/fnhum.2016.00101

Lotze M, Ladda AM, Roschka S et al (2017) Priming hand motor training with repetitive stimulation of the fingertips; Performance gain and functional imaging of training effects. Brain Stimul 10:139–146. https://doi.org/10.1016/j.brs.2016.10.004

Mihai PG, Otto M, Domin M et al (2016) Brain imaging correlates of recovered swallowing after dysphagic stroke: a fMRI and DWI study. NeuroImage Clin 12:1013–1021. https://doi.org/10.1016/j.nicl.2016.05.006

Mori S, Wakana S, Van Zijl PCM, Poetscher L (2005) MRI atlas of human white matter. Elsevier, Amsterdam

Park H-J, Kim JJ, Lee S-K et al (2008) Corpus callosal connection mapping using cortical gray matter parcellation and DT-MRI. Hum Brain Map 29:503–516. https://doi.org/10.1002/hbm.20314

Rittner L, Freitas PF, Appenzeller S, Lotufo R de A (2014) Automatic DTI-based parcellation of the corpus callosum through the watershed transform. Rev Bras Eng Biomed 30:132–143. https://doi.org/10.1590/rbeb.2014.012

Schulz R, Koch P, Zimerman M et al (2015) Parietofrontal motor pathways and their association with motor function after stroke. Brain 138:1949–1960. https://doi.org/10.1093/brain/awv100

Skranes J, Vangberg TR, Kulseng S et al (2007) Clinical findings and white matter abnormalities seen on diffusion tensor imaging in adolescents with very low birth weight. Brain 130:654–666. https://doi.org/10.1093/brain/awm001

Sotiropoulos SN, Jbabdi S, Xu J et al (2013) Advances in diffusion MRI acquisition and processing in the human connectome project. Neuroimage 80:125–143. https://doi.org/10.1016/j.neuroimage.2013.05.057

Wahl M, Hübers A, Lauterbach-Soon B et al (2011) Motor callosal disconnection in early relapsing-remitting multiple sclerosis. Hum Brain Map 32:846–855. https://doi.org/10.1002/hbm.21071

Wassermann EM, Fuhr P, Cohen LG, Hallett M (1991) Effects of transcranial magnetic stimulation on ipsilateral muscles. Neurology 41:1795–1795. https://doi.org/10.1212/WNL.41.11.1795

Witelson SF (1989) Hand and sex differences in the isthmus and genus of the human corpus callosum: a postmortem morphological study. Brain 112:779–835